Energy Transport in Peptide Helices: A Comparison between High- and Low-Energy Excitations

Ellen H. G. Backus,[†] Phuong H. Nguyen,[§] Virgiliu Botan,[†] Rolf Pfister,[†] Alessandro Moretto,[‡] Marco Crisma,[‡] Claudio Toniolo,[‡] Gerhard Stock,[§] and Peter Hamm*,[†]

Physikalisch-Chemisches Institut, Universität Zürich, Winterthurerstrasse 190, CH-8057 Zürich, Switzerland, Institute of Biomolecular Chemistry, Padova Unit, CNR, Department of Chemistry, University of Padova, via Marzolo 1, I-35131 Padova, Italy, and Institut für Physikalische und Theoretische Chemie, J. W. Goethe Unversität, Max-von-Laue-Strasse 7, D-60438 Frankfurt, Germany

Received: November 20, 2007; Revised Manuscript Received: February 19, 2008

Energy transport in a short helical peptide in chloroform solution is studied by time-resolved femtosecond spectroscopy and accompanying nonequilibrium molecular dynamics (MD) simulations. In particular, the heat transport after excitation of an azobenzene chromophore attached to one terminus of the helix with 3 eV (UV) photons is compared to the excitation of a peptide C=O oscillator with 0.2 eV (IR) photons. The heat in the helix is detected at various distances from the heat source as a function of time by employing vibrational pump–probe spectroscopy. As a result, the carbonyl oscillators at different positions along the helix act as local thermometers. The experiments show that heat transport through the peptide after excitation with low-energy photons is at least 4 times faster than after UV excitation. On the other hand, the heat transport obtained by nonequilibrium MD simulations is largely insensitive to the kind of excitation. The calculations agree well with the experimental results for the low-frequency case; however, they give a factor of 5 too fast energy transport for the high-energy case. Employing instantaneous normal mode calculations of the MD trajectories, a simple harmonic model of heat transport is adopted, which shows that the heat diffusivity decreases significantly at temperatures initially reached by high-energy excitation. This finding suggests that the photoinduced energy gets trapped, if it is deposited in high amounts. The various competing mechanisms, such as vibrational T_1 relaxation, resonant transfer between excitonic states, cascading down relaxation, and low-frequency mode transfer, are discussed in detail.

Introduction

Energy transport through molecular systems has received considerable interest in particular due to its importance in molecular electronics and the functioning of biological systems. For example, experimentally, the energy transport through long-chain hydrocarbon molecules,[1] small molecules in solution,[2] and bridged azulene–anthracene compounds[3] has been studied. Also the energy transport in biological systems, such as micelles,[4] reverse micelles,[5] and proteins,[6–18] has been investigated from both an experimental and theoretical point of view. In spite of these efforts, the role of specific protein structural elements (like α-helices and β-sheets) in the energy transport is still not well understood. As α-helices often span the whole protein, it has been speculated that helices channel vibrational energy through biomacromolecules.[19] To test this hypothesis, we have recently studied both experimentally and theoretically the transport of energy through a short but stable peptide 3_{10}-helix.[20] To deposit a large amount of energy in the molecule, a chromophore (an azobenzene-moiety) was attached to the helix, which is electronically excited at ~425 nm (i.e., from the *n* to the π* state) and dissipates this photon energy on an ultrafast time scale after internal conversion (via *cis–trans* isomerization) of the chromophore. We found experimentally that the heat travels through the backbone of the helix with a diffusivity of 2 Å^2 ps^{-1}.

Supplementary molecular dynamics (MD) simulations revealed a 5 times higher diffusivity (10 Å^2 ps^{-1}). We assigned this difference to a "too rigid" force field in the simulations and suggested that it would be interesting to perform experiments with low-energy excitation.[20] Following this line, in this article we compare the energy transport through the helix after excitation with high-energy (~400 nm) light by optically exciting the chromophore with that with low-energy (~6 μm) light by direct excitation of various C=O groups. This procedure lowers the energy deposited into the molecule by a factor 14.

The stable octapeptide 3_{10}-helix[21] consists of seven Aib (α-aminoisobutyric acid) residues, a natural but noncoded amino acid, and one L-Ala residue. Carbonyl groups in the helix are employed as local thermometers, making use of an effect that has been described in detail in ref 22: vibrational transitions become broader and shift to lower frequency upon heating, as a result of anharmonic coupling to thermally excited lower frequency modes. To be site-sensitive, we prepared peptides with a ^{13}C=O labeled Ala (which is more readily available commercially than ^{13}C=O–Aib) at different locations in the amino acid sequence, of which the vibrational frequency is shifted to the red compared to that of the Aib residues. The amino acid Ala is believed not to destabilize the 3_{10}-helix significantly, which has been confirmed by MD simulations as well as by NMR and IR spectroscopy.[20] More specifically, we synthesized two different molecules: one with the ^{13}C=O labeled Ala as the second residue (Figure 1) and one with the label at residue 4, counting from the N-terminus of the helix. The isotope shift of approximately −30 cm^{-1} will essentially localize the

---

* Corresponding author.
† Universität Zürich.
‡ University of Padova.
§ J. W. Goethe Unversität.

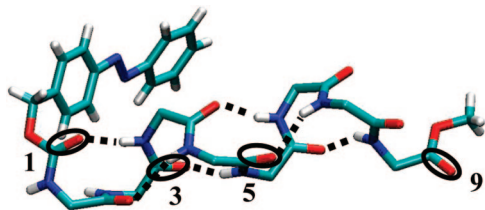**9092** *J. Phys. Chem. B, Vol. 112, No. 30, 2008*

Backus et al.

Figure 1. X-ray diffraction structure of the molecule showing the azobenzene, the urethane connection group, and the peptide helix with the eight residues (seven Aib residues and one [13]C=O-labeled Ala residue). In this work, the Ala residue is either the second or the fourth residue, resulting in the molecules dPAZ-Aib-Ala*-Aib$_6$-OMe (Aib16) and dPAZ-Aib$_3$-Ala*-Aib$_4$-OMe (Aib34), respectively. Amino acid side chains are not shown. The tags refer to the urethane (#1), the labeled peptides (#3 and #5), and the ester (#9) absorption bands in Figure 2.
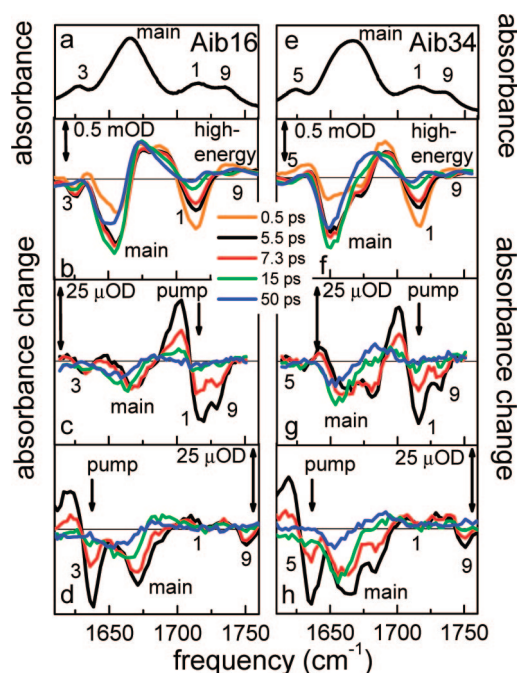

Figure 2. Absorption and transient spectra. (a) IR absorption spectrum of Aib16. (b) Transient signal for Aib16 after high-energy excitation of the azobenzene moiety at 0.5 (orange), 5.5 (black), 7.3 (red), 15 (green), and 50 ps (blue). (c) Transient signal for Aib16 after low-energy excitation of C=O #1 at 5.5, 7.3, 15, and 50 ps. (d) Transient signal for Aib16 after low-energy excitation of C=O #3 at 5.5, 7.3, 15, and 50 ps. (e−h) Same for Aib34. In panel h C=O #5 is pumped. The arrows locate the central position of the IR pump pulse. The measurements are performed at ∼20 °C.

excitation; hence, the isotope labeled amino acid serves as a local thermometer.

At the N-end, a urethane group and an azobenzene moiety are connected to allow pumping with UV light. The azobenzene moiety isomerizes on an ultrafast time scale and thereby locally deposits heat. The flow of heat through the helix was investigated in ref 20 by monitoring the IR response of the ^{13}C-labeled amide groups as well as of the N-terminal urethane and C-terminal methyl ester groups with an IR probe pulse at various times after the excitation. The topic of the present paper is the heat response after low-energy (∼6 μm) excitation of one of the C=O groups. The subsequent heat propagation along the peptide chain is measured by probing the various C=O vibrators.

Materials and Methods

Materials and Experimental Methods. The different laser pulses all originate from a commercial Ti:sapphire amplifier

system. Part of the output was used to generate ∼425 nm light (∼3 μJ, to pump the azobenzene moiety) by frequency doubling used for the high-energy excitation experiments. Infrared pulses (center frequency 1680 cm^{-1}, bandwidth 200 cm^{-1}, energy 1.7 μJ) were produced by difference frequency generation in a AgGaS$_2$ crystal of signal and idler pulses. These were generated by a white-light-seeded two-stage BBO optical parametric amplifier[23] pumped by another part of the output of the Ti:sapphire amplifier. A small fraction of the infrared pulses was split off to obtain broadband probe and reference pulses. The remainder, which was used as a pump pulse in the low-energy excitation experiments, was passed through a computer-controlled Fabry−Perot filter to generate narrow band pump pulses (bandwidth ∼13 cm^{-1}, estimated energy 80 nJ/pulse) to excite a particular C=O group of the helix. With the broadband probe pulse, all C=O oscillators were detected at once. The pump and probe pulses were focused in the sample in spatial overlap. The reference pulse was focused roughly 0.5 mm away. Both probe and reference pulses were frequency dispersed in a spectrometer and detected with a 2 × 63 pixel HgCdTe detector array resulting in a resolution of ∼3 cm^{-1}. The UV or IR pump pulse was delayed with respect to the probe pulse by an optical delay line. All beams were polarized parallel.

The two peptides used in this study are dPAZ-Aib-Ala*-Aib$_6$-OMe (Aib16) and dPAZ-Aib$_3$-Ala*-Aib$_4$-OMe (Aib34), where the asterisk (*) indicates [13]C=O labeling, dPAZ is an abbreviation for fully deuterated 4-(phenyldiazenyl-benzyloxycarbonyl) and OMe stands for methoxy. Deuterated PAZ-Aib-OH was synthesized by nitrating toluene-D$_8$ to *p*-nitrotoluene, oxidizing to *p*-nitrobenzoic acid, reducing with zinc to *p*-aminobenzoic acid, and then making the methyl ester using methanol and thionyl chloride. Reduction of the ester with lithium−aluminum−deuteride[24] leads to the full deuterated *p*-aminobenzyl alcohol. Nitrosobenzene-D$_5$ was obtained by reduction of nitrobenzene-D$_5$ as described in ref 25. Coupling these two deuterated compounds and covalently linking the resulting alcohol to L-Ala* and Aib was performed as reported in refs 26 and 27. Peptide synthesis was performed in solution by activating the carboxyl function with 1-(3-dimethylaminopropyl)-3-ethylcarbodiimide and 7-aza-1-hydroxy-1,2,3-benzotriazole.[28] For details of the peptide synthesis and the characterization of the molecules by IR, NMR, and X-ray diffraction, we refer to ref 20.

The helical peptide was dissolved in chloroform (∼5−10 mM), an apolar and weakly interacting solvent, to minimize heat transport into the solvent. The sample was kept between 2-mm-thick CaF$_2$ windows separated by a 100 μm spacer for the low-energy excitation and the Fourier transform infrared (FTIR) experiments. For the high-energy excitation experiments, a closed cycle flow cell was used with a 100 μm spacer. The experiments with low-energy excitation were performed for the molecule in the *trans* azobenzene state, while the experiments with high-energy excitation were performed with the *cis* state of the molecule, as the *cis* to *trans* yield is higher and the isomerization is faster.[29] The *cis* state (up to ∼80%) was prepared by continuously irradiating at 320 nm (full width at half-maximum (fwhm) 70 nm) from a properly filtered Hg-lamp.

Computational Methods. All simulations were performed with the GROMACS program suite.[30] We used the GROMOS96 force field 43a1[31] to model the PAZ-Aib$_8$-OMe peptide and the rigid all-atom model of ref 32 to describe the chloroform solvent (we checked whether heat transport depends on the rigid or flexible representation of the solvent and found only a minor effect). Additional force field parameters for the azobenzene

Energy Transport in Peptide Helices

J. Phys. Chem. B, Vol. 112, No. 30, 2008 **9093**

unit were derived from density functional theory as described in ref 33. Starting with a 3_{10}-helical conformation, PAZ-Aib$_8$-OMe was placed in an octahedral box containing ~700 chloroform molecules. After energy minimization, the system was simulated for 40 ns at NTP equilibrium conditions (1 atm, 300 K). From this equilibrium trajectory, 400 statistically independent conformations were selected for the subsequent nonequilibrium simulations.

As the nonequilibrium MD simulation approach was described in detail in refs 34 and 35, we only briefly summarize the main aspects of the method. In order to model the UV (high-energy) laser-induced photoisomerization process of the azobenzene,[35] we use a minimal model for the N=N torsional potential energy surfaces that diabatically connect the excited-state S_1 of the *cis* isomer with the ground-state S_0 of the *trans* isomer.[35] Starting with 400 statistically independent conformations, at time $t = 0$ the system is instantaneously switched from the ground-state potential to the "diabatic excited-state" potential. Following this nonequilibrium preparation, the system isomerizes along this "excited-state" potential within typically 0.2 ps. Subsequently, the N=N torsional potential is switched back to its ground-state form, and a constant-energy MD simulation is performed up to 100 ps. This rather crude description of the photoexcitation should be justified as long as there is a clear time scale separation between the excitation process and the subsequent relaxation process (see Discussion below).

To model the IR (low-energy) excitation of a local C=O group,[34] we represent the C=O stretch vibration as a harmonic oscillator with the reduced mass $\mu = (m_C + m_O)/m_C m_O$, coordinate $q_{CO} = q_C - q_O - \langle q_{CO} \rangle$, and momentum $p_{CO} = p_C - p_O$. In terms of classical action-angle variables $\{n, \phi\}$, these variables are represented as[36]

$$q_{CO} = \sqrt{2n+1} \sin \phi$$
$$p_{CO} = \sqrt{2n+1} \cos \phi \qquad (1)$$

where the factor 1 accounts for the zero-point energy of the oscillator. To obtain the initial position and momentum of the initially excited C=O, we associate the action n with the initial quantum state of an oscillator, e.g., $n = 1$ for the first excited state. The vibrational phases ϕ are picked randomly from the interval $[0,2\pi]$. This way, an ensemble of the positions and momenta are calculated, which provide a quasiclassical representation of the quantum initial state of the C=O oscillator.

Following the preparation of the nonequilibrium initial conditions described above, two sets of simulations were performed independently for the high- and low-energy excitation cases. The equation of motion was integrated by using a leapfrog algorithm with a time step of 0.2 fs. We employed the particle-mesh Ewald method to treat the long-range electrostatic interaction.[37] The nonbonded interaction pair-list were updated every 10 fs, using a cutoff of 1.4 nm. All simulations were performed at constant energy (NVE ensemble) for 100 ps, and data were collected every 0.02 ps.

Experimental Results

Steady-State Spectra. Figure 2a,e shows the stationary FTIR absorption spectrum of the helical peptides Aib16 and Aib34 in the amide I (mainly C=O vibration) region. Because the band at 1627 cm^{-1} is not visible in a FTIR absorption spectrum of the peptide with all ^{12}C-Aib residues (data not shown) and because labeling leads to lower frequency, this band is assigned to the isotopically labeled group in the helix, C=O #3 for Aib16 or #5 for Aib34, respectively. The two bands at 1714 and 1735

cm^{-1} can be assigned to the C=O groups from the urethane moiety connected to the azobenzene (C=O #1) and from the ester group of the C-terminal Aib residue (C=O #9), respectively. These two C=O groups are shifted with respect to the others due to their $-C(=O)O-$ nature. The intense band at 1665 cm^{-1} is attributed to all other nonisotope labeled peptide $-C(=O)NH-$ groups (six in total) and is herein called the "main band".

High-Energy Excitation. The heat response of the helix after exciting the azobenzene moiety with high-energy (UV) photons has been discussed in detail in our recent paper.[20] Nevertheless, in order to facilitate the comparison with the low-energy excitation, we shortly repeat the essential results here. The photoexcited azobenzene undergoes an internal conversion (*cis–trans* isomerization) on a 200 fs time scale.[29] When the photon energy (~3 eV) has been distributed over the vibrational degrees of freedom of the azobenzene, an energy equivalent to a local temperature of ~1150 K is estimated right after the photoreaction, assuming the system is thermalized and all energy remains in the azobenzene group. In reality, the temperature will be lower, as part of the photon energy is lost into the solvent as a result of friction during the isomerization process. In particular, the MD simulation predicted a temperature in the photoswitch of ~750 K[20] (however, we will argue below that this number is probably somewhat too low). Nevertheless, these estimates give an idea of the order of magnitude of the effects to be expected. Despite these larges "temperatures", the MD simulation of ref 20 indicated that the helix stays intact on the fast time scale of the experiment.

After photoisomerization of the azobenzene moiety, bands #1 and #3 show instantaneous sharp bleaches (Figure 2b,f), which decay on a 7 ps time scale (gray lines in Figure 3a). These bleaches are due to anharmonic coupling of our spectator modes to thermally excited lower frequency modes and hence can be considered a measure of the amount of vibrational energy in the vicinity of the probe.[22] Note that such a spectral response is obtained, although direct thermal excitation of the spectator modes is extremely unlikely (because of the large vibrational frequency), and also note that this response averages over many low frequency modes, so we cannot deduce whether energy is thermalized. Guided by the MD simulation, we attributed this instantaneous signal to an impact event from the isomerizing azobenzene moiety, where group #3 receives about 1/3 of the energy of group #1. No signal of this sort is observed any further in the helix (bands #5 and #9). After this impact event, heat diffuses from group #1 to group #3.[20] From a simple diffusive rate equation[20] model along the lines of Figure 4 (black arrows), assuming a backward and forward rate of energy transport k_p through low frequency modes and a cooling to the solvent with rate k_s, we deduced for the heat diffusivity $D = k_p \Delta x^2 = 2$ Å^2 ps^{-1} (with $\Delta x \approx 2$ Å being the translation per residue[21]).

The main band responds in a distinctly different way than bands #1 and #3. It grows until ~15 ps, followed by a decay on a 35 ps time scale to roughly 30% of its maximum value (Figure 3b). Bands #5 and #9 only show broad bleaches, which have the same dynamics as the main band. The spectral response between 15 ps and 1 ns is dominated by blue shifts of the corresponding bands. These late-delay-time spectra, for 50 ps delay depicted in the inset of Figure 3b, strongly resemble stationary temperature-induced difference spectra (dotted line in the inset of Figure 3b), suggesting that we are left with the response due to an elevated temperature of the system. The 35 ps decay is a characteristic time scale for heat diffusion from the first solvation shells into the bulk solvent.[38] Note that the
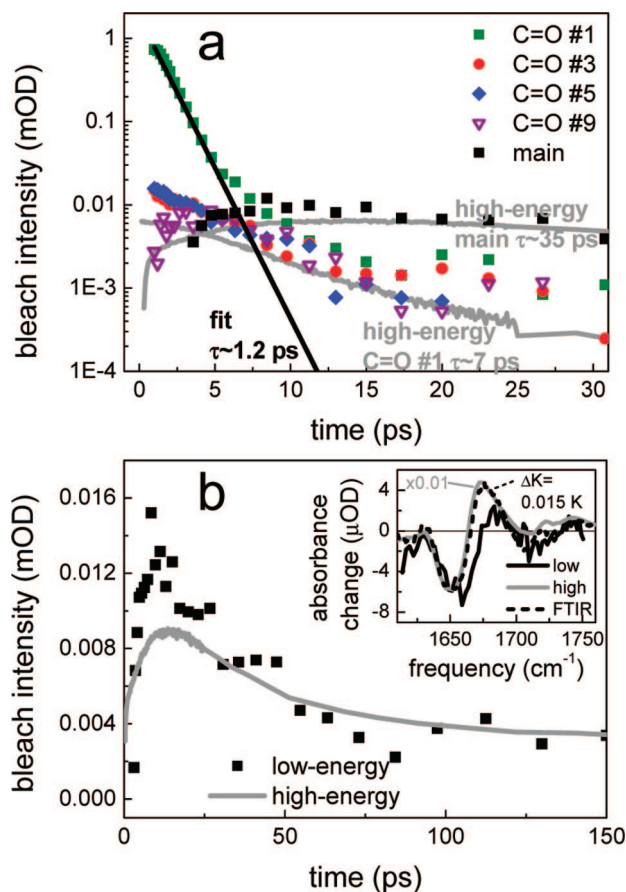
Figure 3. Time traces. (a) The symbols are the bleach intensity (logarithmic scale and with opposite sign as in Figure 2) as a function of time for C=O #1 to #9 and the main band. C=O #1, C=O #3 and the main band are obtained by low-energy excitation of C=O #1 in Aib16 (Figure 2c), C=O #5 is obtained by low-energy excitation of C=O #1 in Aib34 (Figure 2g), and C=O #9 is obtained by low-energy excitation of C=O #3 in Aib16 (Figure 2d). The gray lines are the bleach intensity for C=O #1 and the main band after high-energy pumping (Figure 2b) of the azobenzene moiety in Aib16, both downscaled by a factor 100. The black line is an exponential fit with $\tau = 1.2$ ps of the signal of C=O #1 at early times. If needed, a baseline is subtracted from the data so that all signals for $t > 50$ ps are zero. (b) Bleach intensity as a function of time for the main band after low-energy (black squares) and high-energy (gray line, downscaled by a factor 100) excitation for Aib16 at long delay times. The inset shows the spectra 50 ps after low-energy excitation of Aib16 (black solid line, pumped at C=O #1) and high-energy excitation (gray, downscaled by a factor 100). The dashed line is a stationary temperature-induced difference spectrum of Aib16 corresponding to a temperature jump of 0.015 K.

spectrum at late times, when heat has diffused into the bulk solvent, is given by all molecules in the probe volume, while, at early times, only the molecules excited directly by the laser are probed.

Low-Energy Excitation. For low-energy (IR) excitation, depicted in panels c, d, g, and h of Figure 2, we see remarkable differences at early times compared to the high-energy excitation, while the late-delay-time spectra are rather similar. We therefore discuss the various kinetic components backward in time: the latest time spectra are independent of the excitation frequency (compare the blue curves in panels c and g with those in d and h, respectively) and again represent the elevated temperature of the surrounding solvent. In the inset of Figure 3b, the spectrum at 50 ps has been plotted together with a steady-state difference spectrum with a temperature jump of 0.015 K,[39] revealing remarkable agreement despite the small size of the

signal (8 μOD). Like in the high-energy excitation experiment, the temperature spectrum is largest at about 10 ps, then decays on a ~35 ps time scale until ~100 ps without much change in spectral shape, until it reaches a constant value with an intensity of roughly 1/4 of its maximum (Figure 3b).

At early times (the first few picoseconds) the spectra are dominated by excitation and relaxation of the directly pumped C=O oscillator. The remainder of this signal is still visible in the spectra at 5.5 ps as a strong signal at the pumping frequency, 1716 cm^{-1} (Figure 2c,g) or 1637 cm^{-1} (Figure 2d,h). The vibrational lifetime of C=O vibrators is 1.2 ps (Figure 3a), so after 5.5 ps this signal has decayed enough in amplitude not to obscure other spectral features. It is immediately clear from the spectrum at 5.5 ps that all oscillators feel an effect of the low-energy excitation: bands #1, #3, #5, and #9 all show a sharp bleach, in pronounced difference to the high-energy excitation case (Figure 2b,f). To compare the amplitude and time dependence of the different signals, we plot in Figure 3a the bleach intensities (with opposite sign) of the different bands on a logarithmic scale as a function of time. If needed, a flat baseline was subtracted from the data so that all signals for $t > 50$ ps approach zero. The data for low-energy excitation are depicted as symbols, while the response after high-energy excitation is depicted as gray lines for comparison. Already at 10−15 ps all C=O oscillators have roughly the same amplitude if we excite with low-energy photons, indicating that the energy is equilibrated over the whole molecule. It is immediately clear that the whole set of low-energy excitation data can be described with three time constants: 1.2, 7, and 35 ps. The main band shows a ~35 ps decay time as in the experiments with high-energy excitation, reporting the dissipation of heat from the first solvent shells into the bulk solvent. The oscillator that is pumped (in Figure 3a only C=O #1 is depicted, but we observe the same decay for C=O #3 and C=O #5 if we pump these vibrators) decays biexponentially with a fast component of 1.2 ps, a typical T_1 time for the amide I band.[40,41] At later times, C=O #1 and all other oscillators show a common decay time of ~7 ps (rate k_s in Figure 4). In analogy to ref 20, we assign this signal to excitation of low-frequency modes, to which the C=O vibrators are anharmonically coupled, and its decay to the dissipation of energy out of these low-frequency modes into the surrounding solvent.[42]

From the observation that all C=O groups have roughly the same bleach intensity at 10−15 ps (Figure 3a), a lower limit for heat propagation through the chain can be obtained. We are unable to obtain an upper limit, because the signal up to ~5 ps is dominated by direct excitation of the C=O oscillators. If the process were ballistic, as argued recently by Wang et al.[1] for heat transport through a molecular chain (n-alkanethiol molecules), the velocity is at least ~0.1 nm ps^{-1} (i.e., 6 times 2 Å for each amino acids/15 ps). On the other hand, when we assume diffusive heat transport (such as in the high-energy excitation case,[20] in other theoretical works [6,10] and observed in an indirect way for energy transfer in phospholipid bilayer liposomes [4]), we can extract an estimate of the thermal diffusivity from our rate-equation model schematically depicted in Figure 4. To fully equilibrate heat after 15 ps over all C=O groups, an energy propagation rate of $k_p > (0.5$ ps$)^{-1}$ is needed, corresponding to a thermal diffusivity $D > 8$ Å^2 ps^{-1}. Energy diffusion is thus at least 4 times more efficient after low-energy excitation ($k_p > (0.5$ ps$)^{-1}$) of one of the C=O bands compared to high-energy excitation ($k_p \sim (2$ ps$)^{-1}$) of the azobenzene moiety.

From the amplitudes of the 50 ps spectra, we can estimate that the final temperature in the low-energy excitation experi-

Energy Transport in Peptide Helices

J. Phys. Chem. B, Vol. 112, No. 30, 2008 **9095**

ment is 50 times less than in the high-energy one (taking into account the 2-fold larger concentration in the UV-pump experiment). This result is expected on the basis of the laser pulse intensities (~40 times less pulse energy in the narrow band low-energy pulse compared to the high-energy pulse) and the extinction coefficients (2−3 times lower for one C=O oscillator than for the $n \rightarrow \pi^*$ excitation). The amount of energy per molecule immediately after excitation is ~14 times lower, because the photon energy is 23 500 cm^{-1} (~3 eV) in the high-energy and 1700 cm^{-1} (~0.2 eV) in the low-energy case. Hence, 3 (50 divided by 14) times less molecules are excited in the low-energy pumping case. On the other hand, the signal at early times for group #1, measuring the heat in the helix, is 40−60 times stronger in the high-energy case compared to the low-energy case, which follows from extrapolating the 7 ps component of C=O #1 after low-energy excitation to time zero and compare it to C=O #1 at time zero after high-energy excitation. As this signal at time zero is caused by 3 times more molecules in the high-energy excitation case, we conclude that indeed roughly 14 times more energy per molecule is present in the helix after high-energy excitation than after low-energy excitation (i.e., roughly equalling the ratio of photon energies).

Computational Results

To obtain a microscopic picture of molecular energy transport, we have performed nonequilibrium MD simulations of the high- and low-energy excitation cases. The main results of these simulations are comprised in Figure 5, which shows the time evolution of the kinetic energy per atom of the peptide units along the helix. In the case of high-energy excitation (gray lines), the peak of the photoinduced energy reaches the first unit at about 0.3 ps. The time-delayed rise of the kinetic energies of the subsequent peptide units nicely illustrates the propagation of energy (or heat) along the peptide backbone. Using the simple rate equation model (Figure 4), the time traces can be well fitted by assuming two transport rates, an exchange rate between two peptide units of $k_p = (0.5 \text{ ps})^{-1}$, and a dissipation rate to the solvent of $k_s = (18 \text{ ps})^{-1}$. Compared to the experimental findings, the energy transport along the peptide in simulation is thus about 5 times faster, and the cooling rate is about 2 times slower.[20]

In the case of low-energy excitation (red lines), the kinetic energy of the C=O oscillators is, overall, about a factor of 3 lower than in the case of high-energy excitation. Because of the signal-to-noise ratio obtained from the average over 400 trajectories, the energy transport is hard to extract for distances larger than four peptide units from the excitation. Nevertheless, by using the same rate-equation model (Figure 4), the data can again be modeled with a propagation rate $k_p \sim (0.2-0.6 \text{ ps})^{-1}$ and a cooling time to the solvent of $k_s = (18 \text{ ps})^{-1}$ (black lines in Figure 5). However, it turned out to be necessary to explicitly include the initial, nonthermal, excitation of the high frequency C=O vibrator of group #1 and its $1/T_1$ vibrational relaxation into low frequency modes (see Figure 4) into the fit. Neglecting this first step, the resulting fit of the kinetic energy of unit 1 (indicated by LF) starts significantly too low, while by plotting the sum of populations in both high frequency and low frequency modes (indicated by LF+HF) we obtain almost quantitative agreement. The deviation of the resulting fit of the kinetic energy of unit 2 for times of <1 ps indicates a small direct high-frequency energy transfer between C=O oscillators #1 and #2 (see Discussion).

To compare measured and calculated heat transport under low-energy excitation, Figure 6 shows the time evolution of
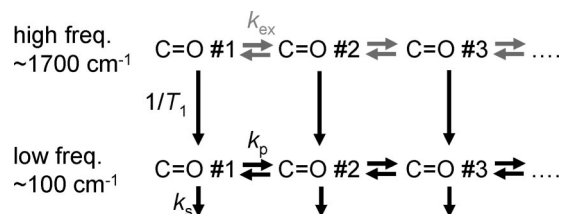

Figure 4. Schematic representation of the energy transport through the molecule. The gray arrows describe direct (excitonic) population transfer with a rate k_{ex}, while the black arrows illustrate energy transport through low-frequency modes with a rate k_p. Cooling to the solvent occurs with rate k_s. The lifetime of the high frequency modes is T_1.
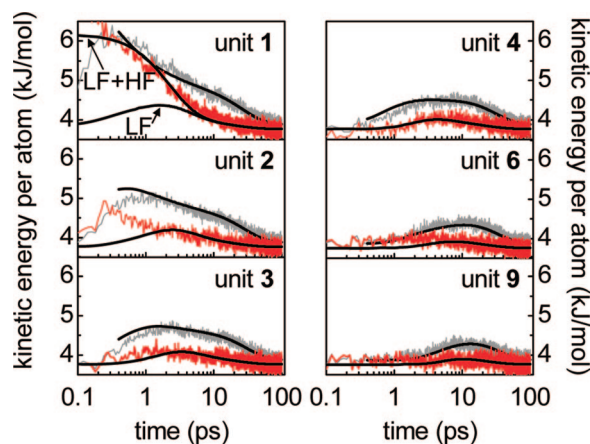

Figure 5. Time evolution of the dynamics of PAZ-Aib$_8$-OMe from the MD simulations. The mean kinetic energy of selected residues after high- (gray) and low- (red) energy excitation is plotted as a function of time. The black lines show global fits according to the model described in the text and for low-energy excitation schematically depicted in Figure 4. After low-energy excitation, the C=O stretch vibration of C=O #1 is excited, a high-frequency (HF) mode. Energy dissipates out of this mode with a time constant of 1.5 ps into low frequency (LF) modes around C=O #1. Subsequently, energy transport through the peptide units takes place with a time constant of 0.4 ps. Cooling to the solvent occurs on a 18 ps time scale.

the bleach amplitude of the sites C=O #3 and #5 normalized to the amplitude of C=O #1 as well as the corresponding calculated result.[43] These ratios start out at zero at $t = 0$ since C=O #1 is initially populated (but not yet C=O #3 and #5), and trend to 1 as population equilibrates throughout the helix. Both experimental and calculated curves are seen to rise on the same time scale and in a similar fashion. For times larger than 10 ps, the signal-to-noise ratio hampers a detailed comparison. Nevertheless, it is clear that the agreement of theory and experiment is clearly better for low- than for high-energy excitation.

Discussion

Several of the results presented above appear surprising on a first account. In particular, our experiments have shown that the energy transport is significantly more efficient for low-energy excitation (although there is much less energy available) than for high-energy excitation. On the other hand, the MD calculations have revealed quite similar energy propagation rates in both cases. Two obvious differences come into one's mind for the two excitation scenarios: (a) In contrast to UV pumping, in the low-energy pump experiment we start with a direct excitation of C=O vibrations, which may delocalize significantly and form excitonic states. (b,c) The energy deposited in the UV-pump case is considerably larger. We will discuss in the following how these effects could affect energy transport.
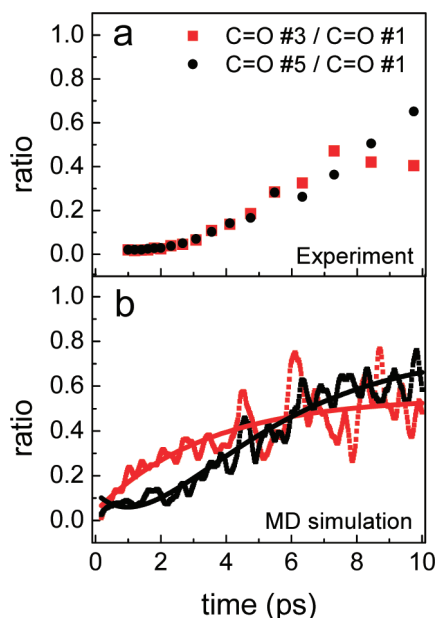
Figure 6. Comparison between experimental signals (low-excitation case) and simulation results. Shown are (a) the signals of sites C=O #3 (red) and C=O #5 (black) normalized to C=O #1 as well as (b) the corresponding calculated site-specific kinetic energy ratios.[43] For better comparison, the calculated rough data (dashed lines) were fitted by biexponential functions (full lines).

(a) Excitonic Transport. It is well established that C=O vibrators in regular peptide structures form excitonic states that can be delocalized significantly.[44–46] In contrast to the high-energy excitation experiment, we directly excite these C=O vibrators in the present experiment. We therefore need to discuss to what extent excitonic coupling may facilitate energy transport, before T_1 relaxation randomizes energy. Excitonic coupling may contribute in two ways. First, the C=O excited-state might delocalize significantly so that vibrational energy would be present throughout the helix right after pumping. Typical excitonic through-space couplings in peptide helices are on the order of a few wavenumbers (e.g., in the case of an α-helix, the couplings have shown to be ∼5 cm^{-1} [47]). To obtain an estimate of the associated delocalization, we have employed a model exciton Hamiltonian,[46] which assumes 5 cm^{-1} for nearest and next-nearest neighbor couplings and chooses diagonal site frequencies in order to reproduce the measured IR spectrum. For an isotope shift of approximately −30 cm^{-1}, we find that the excitation of the labeled C=O group localizes to about 96%. The same is true for group #9, which blue-shifts by about 70 cm^{-1} as a result of its different chemical nature (i.e., an ester group), thus yielding a localization of 99%. Furthermore, the spatial overlap of both eigenstates is negligible, and direct excitonic transport between, e.g., group #3 and #9 (open triangles in Figure 3) seems very unlikely.

The second way in which exciton coupling might contribute is through dissipative energy transport between C=O vibrators directly (i.e., gray arrows and rates k_{ex} in Figure 4). For one of the smallest possible building unit, trialanine, a typical time scale of this direct hopping process between two essentially localized states of 5−15 ps has been reported;[40] too slow to efficiently compete with T_1 relaxation. However, in the present case, two localized states are bridged by the main band, which consists of six largely delocalized states. It has in fact been shown that energy dissipation within delocalized excitonic states can be very efficient on a 500 fs time scale.[48] The dissipation of a localized state into such a bridge of delocalized excitonic states,

and out of it, has not thoroughly been studied yet. Nevertheless, along the lines of Andersen localization,[49] the spatial overlap for both transfer steps is still small, and therefore presumably inefficient (further theoretical studies will be needed to ultimately rule out the contribution of excitonic coupling between C=O states as a possible pathway of energy transport). Hence, we assume that heat transport goes predominantly through low frequency modes after T_1 relaxation is finished. Similar conclusions were drawn by Kurochkin et al.[50] for energy transport between C−N and C=O oscillators in small organic molecules. This hypothesis is also supported by our MD simulations, which showed only a small contribution of excitonic transfer from group #1 to #2 (see Figure 5).

(b) Nonlinear Diffusion Equation. Consider the one-dimensional heat diffusion equation:

$$\frac{dT}{dt} = D_T \frac{d^2 T}{dx^2} \tag{2}$$

which can be regarded as a continuous version of the rate-equation model introduced above. The usual derivation of this theory assumes that the energy gradients ΔT are much smaller than the background temperature T. Only in this limit the thermal diffusivity D_T is independent of temperature during heat propagation, revealing the linear regime of the heat diffusion equation (which is the regime normally considered). For low-energy excitation we presumably are in this regime $\Delta T \ll T$. However, after high energy excitation, the temperature jumps can easily approach the background temperature $\Delta T \approx T$. To study the temperature dependency of the thermal diffusivity, we adopt a simple harmonic model of one-dimensional diffusive transport as pursued by Yu and Leitner[10] and others.[51] Within this theory, the thermal diffusivity can be written as

$$D_T = \frac{\int d\omega \rho(\omega) c(\omega) D(\omega)}{\int d\omega \rho(\omega) c(\omega)} \tag{3}$$

where $\rho(\omega)$ is the density of normal modes, $c(\omega)$ is the contribution of a particular normal mode to the total heat capacity (depending on the occupation of a particular normal mode), and $D(\omega)$ is the contribution of that normal mode to energy diffusion. This expression can be interpreted as a weighted sum over all contributions $D(\omega)$ to the total diffusivity, where $\rho(\omega)c(\omega)$ is the weighting factor. Of this three parameters, only the heat capacity per normal mode $c(\omega)$ is strongly temperature dependent

$$c(\omega) = \frac{(\hbar\omega)^2}{k_B T^2} \frac{e^{\beta\hbar\omega}}{(e^{\beta\hbar\omega} - 1)^2} \tag{4}$$

with $\beta = 1/k_B T$. This function increases strongly with temperature until it reaches the classical limit at $k_B T \approx \hbar\omega$, with a steeper slope for lower frequency modes. Therefore, higher-frequency modes become more important for the thermal diffusivity at higher temperatures in a relative sense. However, these high-frequency modes have a smaller diffusivity, because they tend to be more localized.[10] Therefore, the thermal diffusivity D_T decreases with temperature.

To estimate the magnitude of this temperature dependency, we have performed instantaneous normal mode calculations [52,53] using our nonequilibrium MD trajectories. Figure 7 shows the resulting density of normal modes pertaining to the photoswitchable peptide

Energy Transport in Peptide Helices

J. Phys. Chem. B, Vol. 112, No. 30, 2008 **9097**

$$\rho(\omega) = \rho_0 \sum_{r=1}^{N_{traj}} \sum_{k=1}^{N_{mod}} \int dt \delta(\omega - \omega_k^{(r)}(t)) \qquad (5)$$

averaged over all normal modes ω_k, trajectories r, and times t between 1 and 10 ps (in total, 50 000 snapshots were taken into account). As typically found for peptides, $\rho(\omega)$ shows a pronounced low-frequency band as well as the signatures of various bond stretching modes with frequencies between 1000 and 2000 cm^{-1}. Of particular interest here are instantaneous normal modes with imaginary frequency, which are represented in Figure 7a by negative values of the frequency. Depending on the instantaneous conformation of the molecule, these modes account for unbound motion on inverted parabola and therefore reflect (within the limits of instantaneous normal mode theory[54]) the transport properties of the system. The typical frequency of 100−200 cm^{-1} obtained for these modes agrees well with the frequency of strongly delocalized modes in proteins.[10] To obtain an estimate of the diffusion constant $D(\omega)$ in eq 3 we therefore assume that only normal modes below a certain cutoff frequency ω_C contribute to $D(\omega)$ and approximate $D(\omega)$ by a simple step function with values of 1 below ω_C and 0 above it.[55] The cutoff frequencies used are ω_C = 50, 100, and 200 cm^{-1} in this case study, representing situations where different sets of normal modes are important for the thermal diffusivity. Figure 7b shows the resulting thermal diffusivity D_T plotted as a function of temperature. As expected from the discussion above, we find that D_T significantly decreases with temperature. Assuming UV excitation with an initial temperature of 600 K, the thermal diffusivity may be reduced to ∼50% of its value at 300 K. Hence, the temperature dependence of D_T may explain the 2-fold reduction in the heat transport. This is a significant factor but not quite the factor of >4 we observe for the ratio of the low- and high-energy excitation case experimentally.

(c) Intrasite Relaxation Preceding Energy Transport. However, this factor of 2 in D_T might just be a lower limit of the observed excitation energy dependence of heat transfer. The heat diffusion equation (eq 2) implicitly assumes, by the very use of the concept of a local temperature, that the hot site thermalizes instantaneously as energy flows out through its lower frequency part of the spectrum. In other words, eq 2 implicitly assumes that thermalization *within* one individual peptide unit is significantly faster than thermalization *between* units. However, with a hopping rate between adjacent sites as fast as k_p = (0.5 ps)$^{-1}$, this is hardly possible. In fact we know, for example, that the depopulation rate of the initially excited C=O vibration is $1/T_1$ = (1.2 ps)$^{-1}$, and similar time scales are expected for subsequent relaxation steps as energy cascades down[56,57] from higher to lower energy states within one peptide unit.

The difference between the two scenarios is illustrated in Figure 8. In either case, energy is deposited at site #1; however, at low excitation levels (Figure 8a), this does not lead to significant changes of thermal population. In contrast, after high-energy excitation (Figure 8b), higher-frequency states, which tend to be localized, get thermally excited at a temperature that locally exceeds that of the surrounding by a large amount. As these localized modes hardly contribute to energy transfer, the subsequent relaxation cascade (rate k_c in Figure 8b) to delocalized low-frequency modes may represent the rate-limiting step rather than hopping from site to site k_p.[56,57] However, we wish to stress that the two relaxation processes k_c and k_p, which at a first sight might appear to be distinctly different, might actually have the same physical origin. At the low excitation levels of the IR experiment, on the other hand, repopulation between vibrational modes does not really occur (Figure 8a),
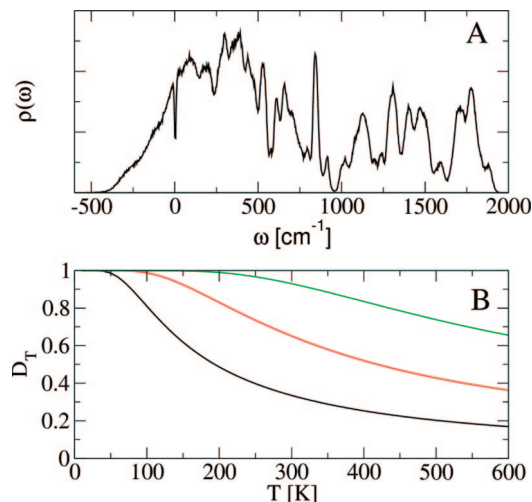

Figure 7. (A) Density of normal modes $\rho(\omega)$ of the photoswitchable peptide as obtained from instantaneous normal mode calculations using nonequilibrium MD trajectories. Instantaneous normal modes of imaginary frequency are represented by negative values of ω. (B) Thermal diffusivity D_T as a function of temperature, calculated from eq 3 using the instantaneous normal modes calculation. As further explained in the text, the frequency-dependent diffusion constant $D(\omega)$ was approximated by a step function with cutoff frequency (black) 50, (red) 100, and (green) 200 cm^{-1}.
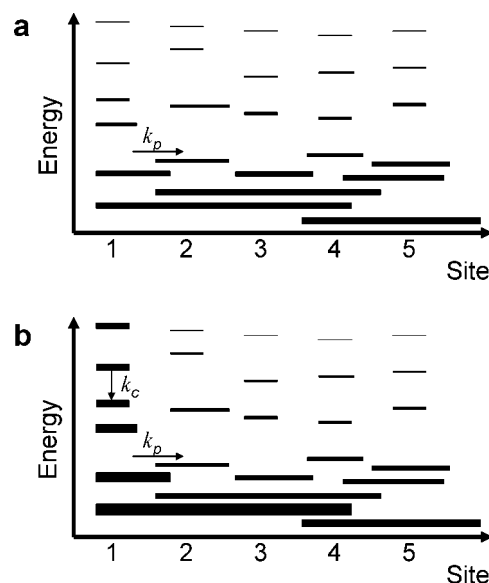

Figure 8. Sketch of "thermal self-trapping". Comparing (a) low-energy and (b) high-energy excitation, vibrational energy levels and their localization/delocalization over various sites are shown. The thickness of each line represents the population of the corresponding state. In either case, energy is deposited at site 1. At low excitation levels (a), this does not lead to significant changes of thermal population. In contrast, after high-energy excitation (b), high-frequency vibrational states, which tend to be localized, get thermally excited at a temperature that locally exceeds that of the surrounding by a large amount. Cascading of this energy down to the conducting low frequency modes with rate k_c might then be the rate limiting step in energy transport (i.e., if $k_c < k_p$). The two relaxation processes k_c and k_p might have the same physical origin.

and cooling within the individual peptide units will not be rate-limiting. We are currently developing an idealized model along the lines of Figure 8, trying to reproduce this effect and understand it in more detail.

We now turn to the discussion of the MD results, which were found to be surprisingly insensitive with respect to the excitation

energy. This finding is, at least in part, also explained by the above-discussed temperature dependence of D_T, which resulted from the quantum-mechanical calculation of the specific heat. In classical MD simulations, however, the heat capacity per normal mode, $c(\omega)$, is constant with temperature. Consequently, following eq 3, the thermal diffusivity D_T will be essentially temperature independent, and the heat diffusion in eq 2 will be linear even under conditions of high-energy excitation.

Furthermore, the MD simulations underestimate the amount of energy arriving in the helix after high-energy excitation. Although high-energy excitation of the azobenzene moiety deposits 14 times more energy in the molecule than direct low-energy excitation of the first C=O group, the difference of kinetic energy for unit #3 to #9 is only ~3 times higher in the MD case (Figure 5). Hence, a significant amount of the energy deposited in the azobenzene moiety does not reach the peptide but dissipates directly into the solvent during the isomerization process.[20] In contrast, from the experiments we deduce that the factor 14 of the photon energies indeed remains once the energy arrives in the helix. Compared to experiment, the calculated energy loss during isomerization of the azobenzene moiety is therefore significantly larger, which most likely is due to our simple model employed to describe the initial *cis–trans* photoisomerization of azobenzene. Disregarding virtually all aspects of multidimensional nonadiabatic photodynamics,[58] our simplistic ansatz to initially deposit the entire photon energy in the central N=N torsion of azobenzene naturally effects that a large fraction of the initial energy is transferred directly into the solvent. To obtain a more realistic modeling of the initial step, true nonadiabatic *ab initio* MD simulations are required.[59–61]

Conclusion

In the present paper, we have compared energy transport through a model peptide helix after high- and low-energy excitation in a combined experimental–computer simulation study. In the first case, energy is deposited through a photochemical reaction, whereas direct vibrational excitation has been used in the second case. This difference has not only a consequence for the amount of energy deposited, but also the form in which it is provided. Whereas energy is offered in an at least randomized, if not thermalized, form starting from the very beginning because of the impact of the isomerizing azobenzene-moiety on the helix,[20,22] the excitation process is mode specific in the second case. The concept of a local temperature becomes applicable only once energy is thermalized, which actually limits the effective time-resolution of the IR-pump experiment to a time scale dictated by the T_1 lifetime of the initially excited vibrator.

In our experiments, we find that energy transport occurs at least 4 times more efficiently after low-energy excitation of a C=O group than after high-energy excitation of the azobenzene moiety. For IR excitation, we deduce a thermal diffusivity of ~8 Å^2 ps^{-1} (or larger), in good agreement with experimentally and theoretically established values.[6,9–11] We attribute the excitation-energy dependence of heat transport to three possible effects: (a) In the low energy experiment, C=O modes are excited directly, which may transport energy through excitonic coupling before T_1 relaxation is complete. Although appearing unlikely at the present stage, we cannot completely rule out this possibility. (b) When thermal gradients within the chain become large, $\Delta T \gg T$, the temperature dependence of the thermal diffusivity can no longer be neglected, and the heat diffusion equation becomes nonlinear. Estimates of the size of this effect, based on the density of normal modes, result in a factor of about two. (c) Thermalization within individual peptide units is not necessarily ultrafast, and may further slow down the process. In particular, in the case of high-energy excitation, localized higher-frequency modes are thermally excited and do not directly contribute to energy transfer, but undergo a subsequent relaxation cascade to delocalized low-frequency modes.

The nonequilibrium MD simulations, on the other hand, did not reproduce the measured excitation-energy dependence of heat transport. We attribute this failure, in part, to the classical nature of the calculations, which results in a temperature-independent specific heat. Consequently, the thermal diffusivity D_T will be essentially temperature independent, too, and the heat diffusion will be linear even under conditions of high-energy excitation. Furthermore, the MD simulation overestimates the initial energy loss into the solvent during photoisomerization process. Most likely, this is due to our simple model employed to describe the nonadiabatic *cis–trans* photoisomerization of azobenzene. We note that both problems of the MD simulations only occur for UV excitation. In fact, the agreement of theory and experiment is clearly better and almost quantitative in the lower energy regime of the IR excitation. Hence, the present study resolves the problem with the unexpectedly low value for thermal diffusivity of ~2 Å^2 ps^{-1} obtained in our previous study for high-energy excitation.[20]

For most biophysical processes, where temperature gradients are expected to be small, the low-energy value of the thermal diffusion constant will be relevant, and the heat diffusion equation will be linear. However, in photobiological processes such as the photoisomerization of retinal in bacteriorhodopsin[62,63] or rhodopsin,[64] the photodissociation of CO from myoglobin,[8,65] or the quenching of excitation energy in antenna complexes by carotenoids,[66] it is not uncommon that the energy equivalent of a visible or UV photon is dissipated into the vibrational system of a protein on an ultrafast subpicosecond time scale, similar to our model system after photoisomerization of the azobenzene moiety. In this case, one might enter a nonlinear regime of heat diffusion, which leads to trapping of energy on a few picosecond time scale: energy gets trapped in localized high-frequency modes by the very form of the Boltzmann distribution (Figure 8b), or, even more so, by a nonthermal distribution in even higher frequency modes. Note that this effect is distinctively different from vibrational self-trapping discussed in the context of Davidov's solitons[19] or vibrational polarons[67,68] in that it does not rely on vibrational anharmonicity in a molecular chain with close to perfect translational symmetry. In fact, the effect described in this paper requires a certain amount of disorder characteristic for glasses and proteins, since only then we are in a situation where low-frequency modes are delocalized and contribute to energy transport, while high-frequency modes are localized. We might call the effect "thermal self-trapping".

References and Notes

(1) Wang, Z.; Carter, J. A.; Lagutchev, A.; Koh, Y. K.; Seong, N.-H.; Cahill, D. G.; Dlott, D. D. *Science* **2007**, *317*, 787.

Energy Transport in Peptide Helices

J. Phys. Chem. B, Vol. 112, No. 30, 2008 **9099**

(2) Wang, Z.; Pakoulev, A.; Dlott, D. D. *Science* **2002**, *296*, 2201.

(3) Schwarzer, D.; Kutne, P.; Schröder, C.; Troe, J. *J. Chem. Phys.* **2004**, *121*, 1754.

(4) Kuciauskas, D.; Wohl, C. J.; Pouy, M.; Nasai, A.; Gulbinas, V. *J. Phys. Chem. B* **2004**, *108*, 15376.

(5) Deàk, J. C.; Pang, Y.; Sechler, T. D.; Wang, Z.; Dlott, D. D. *Science* **2004**, *306*, 473.

(6) Tesch, M.; Schulten, K. *Chem. Phys. Lett.* **1990**, *169*, 97.

(7) Lian, T.; Locke, B.; Kholodenko, Y.; Hochstrasser, R. M. *J. Phys. Chem.* **1994**, *98*, 11648.

(8) Mizutani, Y.; Kitagawa, T. *Science* **1997**, *278*, 443.

(9) Yu, X.; Leitner, D. M. *J. Chem. Phys.* **2005**, *122*, 054902.

(10) Yu, X.; Leitner, D. M. *J. Phys. Chem. B* **2003**, *107*, 1698.

(11) Leitner, D. M. *Adv. Chem. Phys.* **2005**, *130*, 205.

(12) Deàk, J. C.; Chiu, H. L.; Lewis, C. M.; Miller, R. J. D. *J. Phys. Chem. B* **1998**, *102*, 6621.

(13) Miller, R. J. D. *Annu. Rev. Phys. Chem.* **1991**, *42*, 581.

(14) Henry, E. R.; Eaton, W. A.; Hochstrasser, R. M *Proc. Natl. Acad. Sci. U.S.A.* **1986**, *83*, 8982.

(15) Okazaki, I; Hara, Y.; Nagaoka, M. *Chem. Phys. Lett.* **2001**, *337*, 151.

(16) Sagnella, D. E.; Straub, J. E. *J. Phys. Chem. B* **2001**, *105*, 7057.

(17) Nguyen, P. H.; Gorbunov, R. D.; Stock, G. *Biophys. J.* **2006**, *91*, 1224.

(18) Fujisaki, H.; Straub, J. E. *Proc. Natl. Acad. Sci. U.S.A.* **2005**, *102*, 6726.

(19) Davydov, A. S. *Phys. Scr.* **1979**, *20*, 387.

(20) Botan, V.; Backus, E. H. G.; Pfister, R.; Moretto, A.; Crisma, M.; Toniolo, C.; Nguyen, P. H.; Stock, G.; Hamm, P. *Proc. Natl. Acad. Sci. U.S.A.* **2007**, *104*, 12749.

(21) Toniolo, C.; Benedetti, E. *Trends Biochem. Sci.* **1991**, *16*, 350.

(22) Hamm, P.; Ohline, S. M.; Zinth, W. *J. Chem. Phys.* **1997**, *106*, 519.

(23) Hamm, P.; Kaindl, R. A.; Stenger, J. *Opt. Lett.* **2000**, *25*, 1798.

(24) Nystrom, R. F.; Brown, W. G. *J. Am. Chem. Soc.* **1947**, *69*, 2548.

(25) Shine, H. J.; Zmuda, J.; Kwart, H.; Horgan, A. G.; Brechbiel, M. *J. Am. Chem. Soc.* **1982**, *104*, 5181.

(26) Schwyzer, R.; Sieber, P.; Zatsko, K. *Helv. Chim. Acta* **1958**, *41*, 491.

(27) Li, C. H. *Chem. Abstr.* **1963**, *59*, 10239e.

(28) Carpino, L. A. *J. Am. Chem. Soc.* **1993**, *115*, 4397.

(29) Nägele, T.; Hoche, R.; Zinth, W.; Wachtveitl, J. *Chem. Phys. Lett.* **1997**, *272*, 489.

(30) Lindahl, E.; Hess, B.; van der Spoel, D. *J. Mol. Model.* **2001**, *7*, 306.

(31) van Gunsteren, W. F.; Billeter, S. R.; Eising, A. A.; Hünenberger, P. H.; Krüger, P.; Mark, A. E.; Scott, W. R. P.; Tironi, I. G. *Biomolecular Simulation: The GROMOS96 Manual and User Guide*; Vdf Hochschulverlag AG an der ETH Zürich: Zürich, 1996.

(32) Tironi, I. G.; van Gunsteren, W. F. *Mol. Phys.* **1994**, *83*, 391.

(33) Nguyen, P. H.; Mu, Y.; Stock, G. *Proteins* **2005**, *60*, 485.

(34) Nguyen, P. H.; Stock, G. *J. Chem. Phys.* **2003**, *119*, 11350.

(35) Nguyen, P. H.; Stock, G. *Chem. Phys.* **2006**, *323*, 36.

(36) Schinke, R. *Photodissociation Dynamics*; University Press: Cambridge, 1993.

(37) Darden, T.; York, D.; Pedersen, L. *J. Chem. Phys.* **1993**, *98*, 10089.

(38) Phillips, C. M.; Mizutani, Y.; Hochstrasser, R. M. *Proc. Natl. Acad. Sci. U.S.A.* **1995**, *92*, 7292.

(39) The temperature difference used was 10 K and was downscaled to an effective temperature difference of ∼0.015 K. This roughly corresponds to the expected temperature jump in the time-resolved experiment after the pump energy is dissipated completely into the bulk solvent.

(40) Woutersen, S.; Mu, Y.; Stock, G.; Hamm, P. *Proc. Natl. Acad. Sci. U.S.A.* **2001**, *98*, 11254.

(41) Peterson, K. A.; Rella, C. W.; Engholm, J. R.; Schwettman, H. A. *J. Phys. Chem. B* **1999**, *103*, 557.

(42) Dahinten, T.; Baier, J.; Seilmeier, A. *Chem. Phys.* **1998**, *232*, 239.

(43) We assume that the measured relative bleach amplitudes are directly related to the corresponding calculated site-specific kinetic energy ratios $A_n(t) = (E_n(t) - E_n(100\ ps))/(E_1(t) - E_1(100\ ps))$, where $n = 3$ and 5 labels the peptide unit, and the long time limit was subtracted in both experiment and theory.

(44) Krimm, S.; Bandekar, J. *Adv. Protein Chem.* **1986**, *38*, 181.

(45) Torii, H.; Tasumi, M. *J. Chem. Phys.* **1992**, *96*, 3379.

(46) Hamm, P.; Lim, M. H.; Hochstrasser, R. M. *J. Phys. Chem. B* **1998**, *102*, 6123.

(47) Fang, C.; Hochstrasser, R. M. *J. Phys. Chem. B* **2005**, *109*, 18652.

(48) Jansen, T. l. C.; Knoester, J. *Biophys. J.* **2008**, *94*, 1818.

(49) Anderson, P. W. *Phys. Rev. B* **1958**, *109*, 1492.

(50) Kurochkin, D. V.; Naraharisetty, S. R. G.; Rubtsov, I. V. *Proc. Natl. Acad. Sci. U.S.A.* **2007**, *104*, 14209.

(51) Allen, P. B.; Feldman, J. L. *Phys. Rev. B* **1993**, *48*, 12581.

(52) Buchner, M.; Ladanyi, B. M.; Stratt, R. M. *J. Chem. Phys.* **1992**, *97*, 8522.

(53) Keyes, T. *J. Phys. Chem. A* **1997**, *101*, 2921.

(54) Gezelter, J. D.; Rabani, E.; Berne, B. J. *J. Chem. Phys.* **1997**, *107*, 4618.

(55) That is, the integral in the nominator of eq 3 is evaluated from 0 to ω_C, while the integral in the denominator is taken from 0 to infinity.

(56) Hill, J. R.; Dlott, D. D. *J. Chem. Phys.* **1988**, *89*, 830.

(57) Rey, R.; Moller, K. B.; Hynes, J. T. *Chem. Rev* **2004**, *104*, 1915.

(58) Stock, G.; Thoss, M. *Adv. Chem. Phys.* **2005**, *134*, 243.

(59) Doltsinis, N. L.; Marx, D. *Phys. Rev. Lett.* **2002**, *88*, 166402.

(60) Toniolo, A.; Ciminelli, C.; Persico, M.; Martínez, T. J. *J. Chem. Phys.* **2005**, *123*, 234308.

(61) Nonnenberg, C.; Gaub, H.; Frank, I *ChemPhysChem* **2006**, *7*, 1455.

(62) Polland, H.-J.; Franz, M. A.; Zinth, W.; Kaiser, W.; Köling, E.; Oesterhelt, D. *Biophys. J.* **1986**, *49*, 651.

(63) Mathies, R. A.; Cruz, C. H. B.; Pollard, W. T.; Shank, C. V. *Science* **1988**, *240*, 777.

(64) Wang, Q.; Schoenlein, R. W.; Peteanu, L. A.; Mathies, R. A.; Shank, C. V. *Science* **1994**, *266*, 422.

(65) Martin, J. L.; Migus, A.; Poyart, C.; Lecarpentier, Y.; Astier, R.; Antonetti, A. *Proc. Natl. Acad. Sci. U.S.A.* **1983**, *80*, 173.

(66) Demmig-Adams, B. *Biochim. Biophys. Acta* **1990**, *1020*, 1.

(67) Scott, A. C. *Phys. Rep.* **1992**, *217*, 1.

(68) Xie, A.; van der Meer, L.; Hoff, W.; Austin, R. H. *Phys. Rev. Lett.* **2000**, *84*, 5435.